Chemical principles of single-molecule electronics

Timothy A. Su[1], Madhav Neupane[1], Michael L. Steigerwald[1], Latha Venkataraman[1,2] and Colin Nuckolls[1]

Abstract | The field of single-molecule electronics harnesses expertise from engineering, physics and chemistry to realize circuit elements at the limit of miniaturization; it is a subfield of nanoelectronics in which the electronic components are single molecules. In this Review, we survey the field from a chemical perspective and discuss the structure–property relationships of the three components that form a single-molecule junction: the anchor, the electrode and the molecular bridge. The spatial orientation and electronic coupling between each component profoundly affect the conductance properties and functions of the single-molecule device. We describe the design principles of the anchor group, the influence of the electronic configuration of the electrode and the effect of manipulating the structure of the molecular backbone and of its substituent groups. We discuss single-molecule conductance switches as well as the phenomenon of quantum interference and then trace their fundamental roots back to chemical principles.

Over the past century, experimental physicists and engineers have developed sophisticated methods to create semiconducting silicon-based devices, such as diodes, transistors and memory elements, of increasingly small dimensions. Meanwhile, chemists have acquired a detailed understanding of the relationship between the chemical structure and the electronic properties of a molecule through reaction chemistry, advanced physical chemistry and theoretical methods. These multidisciplinary efforts have converged in the field of single-molecule electronics (SMEs), in which the ultimate goal is to use molecules as active elements in electronic circuitry[1,2]. A rich knowledge base detailing the electronic properties of molecules already exists in the context of chemical reactivity; reimagining such properties in the framework of SMEs might then inspire tremendous advancements in the field.

Powerful methods have been developed to characterize and manipulate the conductance properties of single molecules[3–6]. Molecular conductance has been measured using techniques based on scanning tunnelling microscopy (STM)[7], mechanically controlled break junctions[8–11], STM break junctions[12,13], conductive atomic force microscopy[14], electromigration[15], nanoparticle arrays[16,17] and other approaches[18–21]. The sophistication of these techniques provides the opportunity for chemists to collaborate with physicists and engineers to incorporate well-understood chemical principles into the study of structure–conductivity relationships in molecular wires.

Reviews on SMEs are usually written from the perspective of those who build devices and measure their properties — the link between chemistry and SME devices is rarely the focus. Filling this gap will address the questions that arise from the expanding structural diversity of molecular wires in the SME literature. For example, how will the single-molecule conductance paradigm, which was first developed for simple molecular structures, shift as molecular wires grow in structural complexity and diversity? Which lessons can be drawn from reaction chemistry to guide the design of molecular electronics? How can chemical expertise be used to engineer new functions into single-molecule wires?

In this Review, we integrate the languages of chemistry and device physics to explain the chemical concepts that underlie single-molecule conductance. We discuss the structure–property relationships of single-molecule junctions by deconstructing the junction into three distinct components: the anchor, the electrode and the bridge (FIG. 1). We survey the modularity of each component and describe how tuning the structure of each part affects the charge-transport properties of the junction, primarily in the context of break-junction experiments. Finally, we examine emerging areas in SME research, such as single-molecule conductance switches and quantum interference (QI), and discuss how these are fundamentally related to well-established chemical principles.

[1]*Department of Chemistry, Columbia University.*
[2]*Department of Physics and Applied Math, Columbia University, New York, New York 10027, USA.*

Correspondence to M.L.S., L.V. and C.N.
mls2064@columbia.edu; lv2117@columbia.edu; cn37@columbia.edu

Arricle number: 16002
doi:10.1038/natrevmats.2016.2
Published online 23 Feb 2016

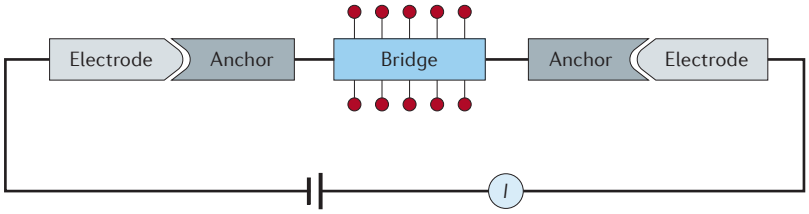

Figure 1 | **A schematic of a single-molecule junction with electrode, anchor and bridge components.** The bridge unit can be further deconstructed into backbone (blue block) and substituent (red circles) subunits. *I*, current.

Anchor group

The anchor group (also known as the linker or contact group) connects the molecular wire to the electrodes both mechanically and electronically. Usually, a single anchoring group terminates each end of the molecule to form the metal–molecule–metal junction; however, including more anchoring units along the molecular bridge can offer additional handles for tuning conductance, depending on which two anchors form the most conductive pathway[22–27]. Anchoring groups typically bind to electrodes either through donor–acceptor (dative) interactions or through covalent bonding. Prototypical anchor groups for each type of electrode–linker interaction are shown in FIG. 2a. Because gold is the most used electrode material in SME studies, we focus primarily on the interaction of anchor groups with gold electrodes.

Dative interactions involve the electron donation from a π donor or a lone pair donor to a Lewis acidic Au atom. Common π donors include fullerenes[28,29] and other π-conjugated hydrocarbons[19,26,30,31]. Many lone pair anchoring groups are common σ-donor ligands familiar from coordination chemistry[32]. Dative contacts, such as amines, are advantageous because they bind selectively to undercoordinated adatoms on the electrode surface; this narrows the conductance distribution because it limits the Au–linker contact geometry[33]. Covalent contacts between the metal and the molecule result from covalent bonding between molecular radicals and metallic electrode surfaces. Covalent contacts are valuable because they are physically robust linkages that strongly couple the electronics of the molecule and the metal.

Conductance depends not only on the class of the anchoring group but also on the nature of the interaction between the anchor group and the other components of the junction — that is, the bridge and the electrode. In the following sections, we explore how the spatial overlap between the orbitals of these three components affects the charge-transport properties of the junction.

Before we continue, we must clarify the meaning of the conductance values that are discussed. There is significant measurement-to-measurement variability in single-molecule experiments that is due to fluctuations in the molecular conformation, the electrode–anchor contact geometry and the electrode surface geometry. To account for this variability and to better understand the nature of conductance in a single molecule, researchers analyse hundreds to thousands of measurement traces together by compiling them into conductance histograms to obtain a distribution of all measured conductance values. The conductance values that we report here refer to the conductance peak values from such histograms reported in units of G_0. G_0 is the conductance quantum and is defined as $G_0 = 2e^2/h = 77.5\ \mu S$, where e is the charge of an electron and h is Planck's constant; it is the preferred unit used to describe the conductance between metal point contacts as well as molecular conductance.

Effect of anchor–bridge orbital overlap on conductance. The anchor group often dictates whether the molecular wire transports holes (highest occupied molecular orbital (HOMO)-dominated conductance) or electrons (lowest unoccupied molecular orbital (LUMO)-dominated conductance). The dominant conducting molecular orbital is typically the orbital that is closest in energy to the electrode Fermi level, E_F. Conductance depends on the energy offset, ΔE, between E_F and the conducting orbital, and on the strength of the electrode–molecule hybridization, Γ (BOX 1). The nature of the conducting orbital can be determined experimentally through thermopower measurements[34,35] or computationally by transmission calculations[36]. However, in simple structures, we can predict the nature of charge carriers from basic chemical principles by considering the nature of the molecular backbone and the geometry of the lone pair relative to the conjugated orbitals of the molecule (FIG. 2b). To illustrate this method, we use a phenyl ring terminated at the *para* positions by the dative linker groups from FIG. 2a. This analysis can be applied to other basic aromatic wires as well. For benzene rings terminated with linkers such as –SR, $–NH_2$, $–PR_2$ or –SeR at the 1,4-positions, the lone pair orbitals are included in the HOMO because they are coplanar with and energetically destabilized by the filled π-conjugated bridge orbitals. Thus, owing to the alignment of the Au–lone pair bonds with the π system of the bridge, conductance occurs strongly through the HOMO when such anchor groups are used.

By contrast, conductance in phenyl rings terminated by pyridine[37], isocyanide[38] and cyanide[39] linkers occurs primarily through the LUMO. For these anchor groups, the lone pair lies in the σ plane of the molecule, rigidly orthogonal to the π channel of the wire. Conduction through the lone pair orbitals is weak because the carbon sp^2 σ orbitals are poorly conjugated[40]. Moreover, the lone pair orbital is generally quite low in energy because it is part of the σ system; thus, transport through this orbital has a marginal contribution to conductance (ΔE is large). Just as importantly, the electron-withdrawing nature of these linker groups facilitates LUMO-dominated conductance by lowering the energy of the π^*-antibonding orbitals towards the E_F (and the HOMO-conducting π-bonding orbitals away from the E_F). The conductance is then controlled by the coupling between the electrodes and the π^*-antibonding orbitals of the LUMO. When molecular bridges are very electron-deficient structures, such as thiophene

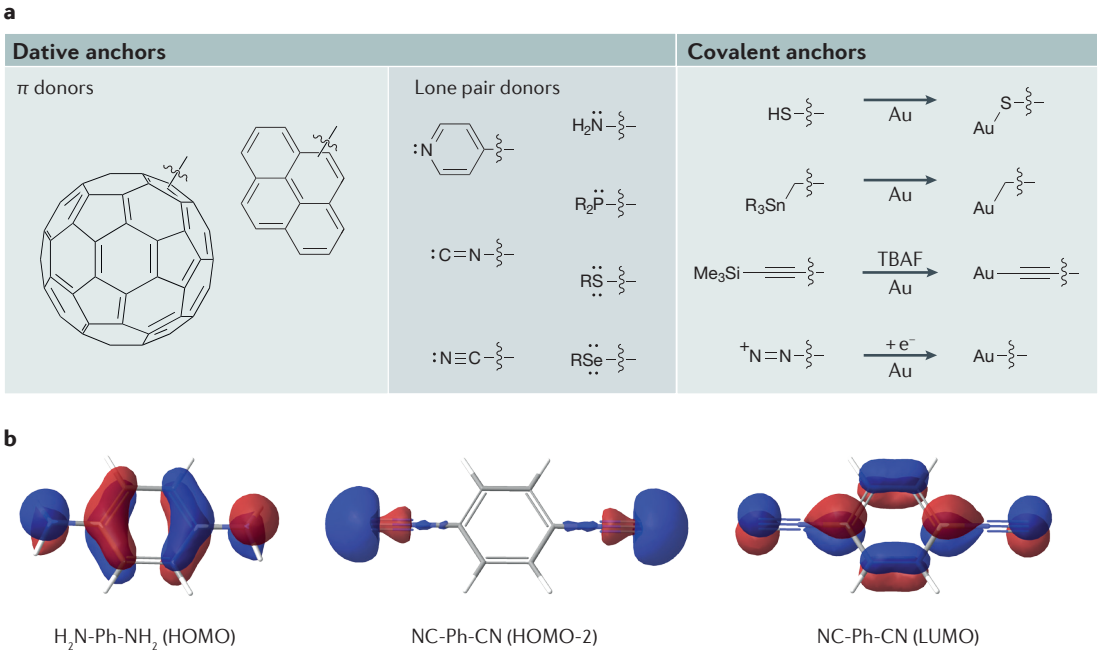

Figure 2 | **Anchor group archetypes and the nature of charge carriers for common dative anchors. a** | Molecular structures of common anchors. Dative anchors can be classified as π donating or lone pair donating. For lone pair donors, the anchors shown in the left and in the right columns impart lowest unoccupied molecular orbital (LUMO)- and highest occupied molecular orbital (HOMO)-dominated conductance, respectively, in simple π-conjugated systems. Covalent anchors commonly used to generate direct Au–S and Au–C contacts are shown in the last column. These contacts can be generated from thiol oxidation, Au–Sn transmetalation, fluoride-initiated desilylation and diazonium electroreduction reactions. **b** | The highest energy molecular orbital surfaces that feature strong lone pair character are depicted for 1,4-diaminobenzene (left panel) and 1,4-dicyanobenzene (middle panel) (B3LYP/6-31G**). In 1,4-diaminobenzene, the N-centred lone pairs occupy *p* orbitals that, like the benzene π orbitals, are perpendicular to the plane of the ring. In 1,4-dicyanobenzene, these N-centred lone pair orbitals are orthogonal to the π channel of the benzene ring; conductance in this system is dominated instead by transport through the LUMO (right panel).

dioxides[41] and porphyrins[42], in which the HOMO and LUMO energies are substantially lowered, conductance through the LUMO can dominate regardless of the type of linker used.

HOMO and LUMO conduction can also be understood from the perspective of coordination chemistry and of the different modes of interaction between ligands and transition metals. Hole transport or HOMO-dominated conduction occurs when the metal–molecule bond, formed using the σ-donor orbital of the molecule (which in most cases is the HOMO of the isolated molecule) and the σ-accepting orbital of the metal, can become coplanar with the conjugated bridge orbitals. This coplanarity ensures that the metal–molecule bond, the 'gateway', can mix with the delocalized, conjugated bridge orbitals and establish the conductivity path. Conversely, if the metal-to-molecule σ bond cannot mix with the conjugated pathway, the charge carriers cannot use the molecular HOMO; it is geometrically unavailable and energetically distant from the E_F. However, it is well known from coordination and organometallic chemistry that although ligand-to-metal σ donation usually dominates metal–ligand bonding, it is often supplemented by d_{metal} to π^*_{ligand} 'back-bonding', in which occupied orbitals of the metal mix with unoccupied orbitals of the ligand. In the case of molecular conduction, when the σ-donation (HOMO-transporting) pathway is unavailable, this π^* back-bonding (LUMO-transporting) pathway may be available if the π^* orbital, into which the metal back-donates, is a conjugated orbital that spans the molecule and is connected to both electrodes.

The stereochemistry of the Au–anchor bond with respect to the conductive channel of the molecular bridge determines the strength of the electronic coupling between the metal and the molecule; manipulating this stereochemistry is a powerful handle for controlling conductance. The charge flow between the electrodes increases if the Au–anchor bond is aligned with the conjugated orbitals of the molecule. The position of sulfur lone pairs can be locked into alignment with the molecular π backbone using a dihydrobenzothiophene (BT) thioether linker[43]. The frustrated rotation of the S lone pair results in increased conductance and in a sharper conductance peak compared with analogous aromatic wires with thiomethyl linkers that can freely rotate. The BT linker has been incorporated into several different molecular wires to strengthen the anchor–bridge coupling[27,44–46].

Poor coupling between the electrode and the molecule can also be a desirable quality. Electrode–molecule coupling can be disrupted by inserting

methylene (CH_2) units between the S atom and the phenyl ring. The methylene spacers allow gating effects, such as Coulomb blockade, to occur in three-electrode systems because they decouple the molecule from the source and drain the electrodes[47] (FIG. 3a). However, the reduction in molecule–electrode coupling has been shown to decrease the junction conductance by three orders of magnitude in π-conjugated molecules[47]. Interesting functions can be implemented into molecular electronic devices by synthetically engineering anchor groups with both strong and weak electrode–molecule coupling character. A bulky –SPh anchor group can be used to misalign the S–Au bond with the molecular bridge, decreasing the molecule–electrode coupling[45]. This enables the creation of a single-molecule rectifier, whereby the molecule is strongly coupled to the electrode by a covalent Au–C bond at one end and weakly coupled by a Au–SPhR bond at the other end. A class of oligosilanes and oligogermanes that switch between different conductance values depending on the strength of the coupling between the electrode and the molecule has recently been described[48,49]. Junction elongation stretches the terminal ends of the molecule into a geometry (*ortho–ortho* (O–O)) that is optimal for conductance and electrode–molecule coupling; junction compression relaxes the molecule into dihedral geometries (*anti–anti* (A–A) or *ortho–anti* (O–A)) with diminished electrode–molecule coupling and lower conductance (FIG. 3b).

In situ *chemical reactions to produce covalent contacts.* Au–S linkages formed from the reduction of thiol (–SH) linkers on Au surfaces are the most widely studied form of covalent contact. Strong Au–S linkages enable the molecular junction to withstand harsh external conditions such as mechanical stress[50] and high-bias voltages[51]. Thiols can oxidize to disulfides rather easily under ambient conditions; this is problematic because dithiolated molecular wires can polymerize and form insoluble polydisulfides[52]. Although S–S bonds can be reduced on gold surfaces[53], there is no guarantee that the reduction will be exhaustive and that only the

Box 1 | **Principles of charge transport in single-molecule junctions**

In the limit of coherent transport, the conductance of a molecular junction is related to the probability of electron transmission between the electrodes through the Landauer formula[143,144]. Often, this transmission probability strongly depends on the extent of the hybridization of a single molecular orbital with the continuous band of energy levels on the metal electrode. In these cases, transmission depends primarily on the energetic alignment (ΔE) of this orbital with respect to the metal Fermi level (E_F) and on the broadening (Γ) of the orbital due to hybridization, which gives electrons on this level a finite lifetime ~$\hbar/\Gamma$. In the figure, the red Lorentzian curves (lowest unoccupied molecular orbital (LUMO)) and blue Lorentzian curves (highest occupied molecular orbital (HOMO)) depict a typical transmission function plotted against energy. The transmission function shown here describes HOMO-dominated conductance because the HOMO transmission peak is closest in energy to and intersects the E_F; a similar picture for LUMO-dominated conductance would show the LUMO transmission peak intersecting the E_F.

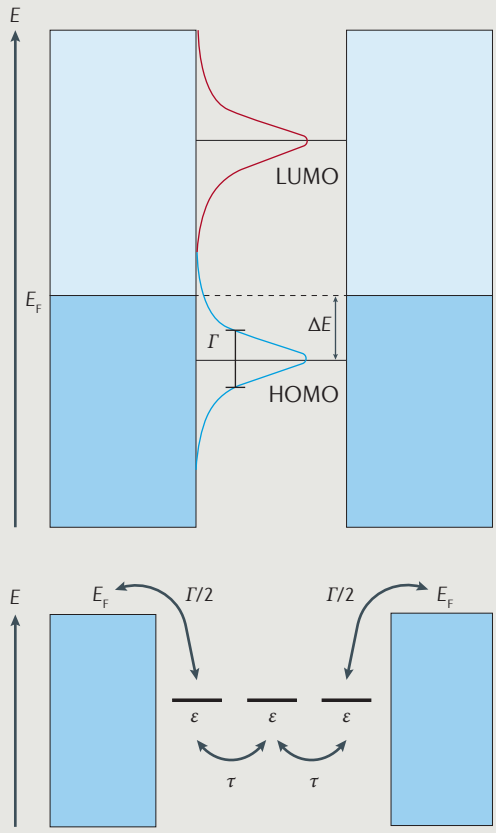

The parameters Γ and ΔE depend on intrinsic molecular and metallic characteristics, including the nature of the molecular orbital, the molecule–metal bond character (covalent or donor–acceptor), the electronic density of states of the metal and the charged interactions at the metal–molecule interface. Orbitals that have density on the metal-binding anchor groups generally result in a broadened transmission resonance (large Γ), whereas those that localize electron density on the molecular backbone show very narrow resonances (small Γ). The length of the molecule also effects the width of the resonance; small molecules, such as H_2 and short π-conjugated wires, are strongly coupled because their orbitals effectively hybridize with the metal, which results in a large Γ. For longer molecular wires, Γ is smaller because a larger proportion of the hybridized orbital is localized on the molecular backbone. In oligomeric materials, Γ decreases with increasing n more quickly if the conjugation or coupling strength (τ) between oligomer units is weak. This is related to the reason why the length-dependent conductance decay parameter (β) is small for conjugated repeat units but large for non-conjugated repeat units. The lower panel of the figure schematically represents a tight-binding model that assigns a single level (ε) to each repeat unit and the parameter τ that describes the electronic coupling between them. The coupling of these units with the electrodes is described by $\Gamma/2$.

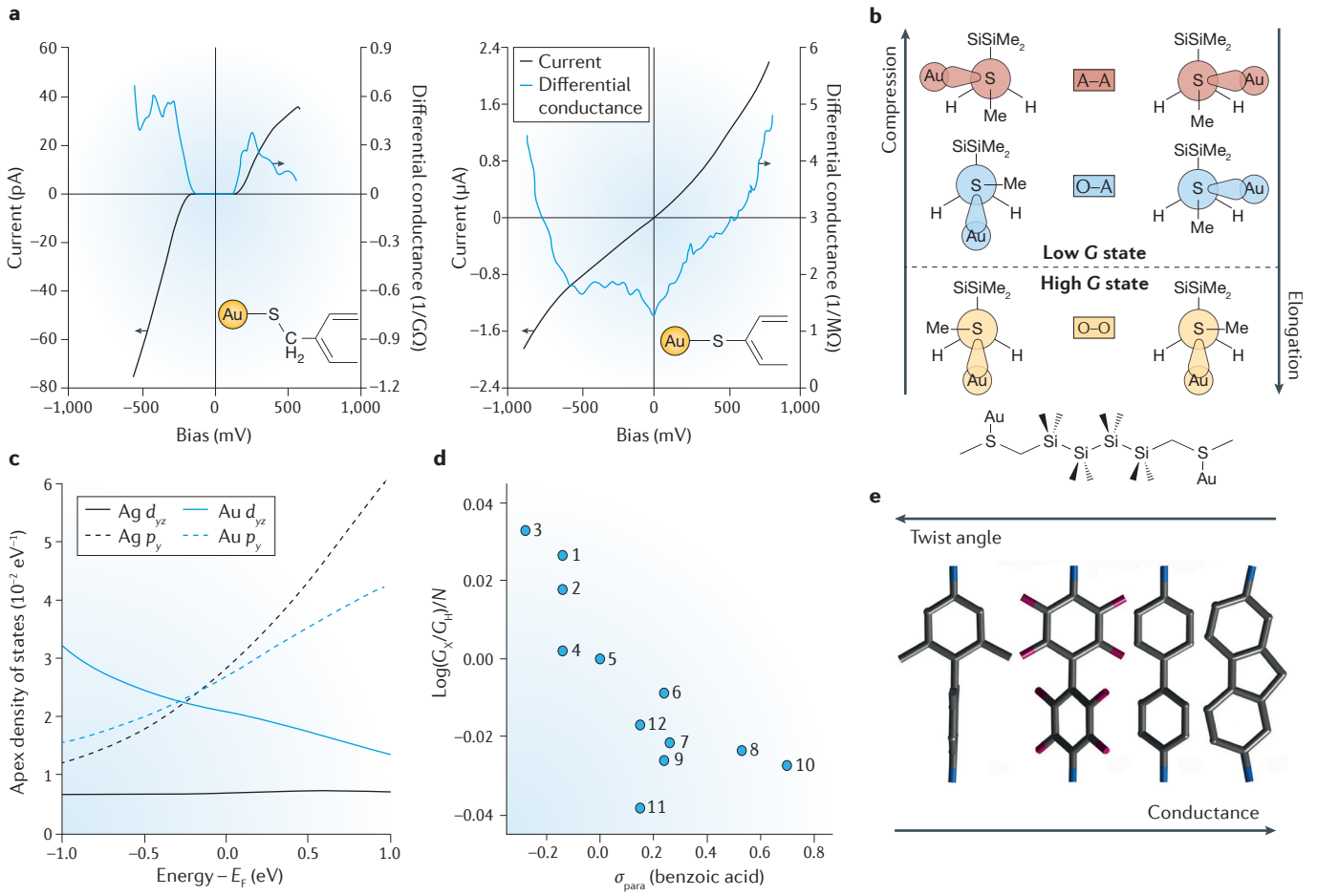

Figure 3 | **Tuning the structure of the anchor, electrode and bridge to modulate charge-transport properties in single-molecule junctions. a** | Current and differential conductance plotted against source-drain voltage bias at a constant 1V gate voltage for an oligo(*p*-phenylene vinylene) molecule with (left panel) and without (right panel) methylene insertions adjacent to the thiol. The tunnelling barrier introduced by the methylene unit decouples the molecule from the electrodes and a Coulomb blockade is observed. **b** | Newman projections depicting the *anti* (A) and *ortho* (O) terminal dihedral conformations in a Au–oligosilane–Au junction. Junction elongation causes the terminal electrode–anchor dihedral geometry to shift from low conducting (low *G* state), with weakly coupled A–A and O–A configurations, to high conducting (high *G* state), with a strongly coupled O–O configuration. **c** | Density of states around the Fermi level (E_F) for p_y and d_{yz} orbitals in Ag and Au. The stronger *d*-orbital character of Au compared with Ag near the E_F results in a stronger d–π^* coupling for pyridine anchors and, therefore, an increased conductance. **d** | The Hammett plot shows the relationship between conductance and each substituent's Hammett coefficient σ_{para} in substituted benzene rings. **e** | Conductance decreases with an increasing twist angle between biphenyl rings. G_H, conductance of unsubstituted molecule; G_X, conductance of substituted molecule; *N*, number of substituents. Panel **a** is adapted with permission from REF. 47, American Chemical Society. Panel **b** is from REF. 48, Nature Publishing Group. Panel **c** is adapted with permission from REF. 92, American Chemical Society. Panel **d** is reproduced with permission from REF. 103, American Chemical Society. Panel **e** is from REF. 13, Nature Publishing Group.

monomers will contribute to conduction measurements. A common approach for increasing the ambient stability of thiol-based wires is to functionalize the thiols with thioacetate-protecting groups that can cleave on the electrode surface to form covalent Au–S contacts[52,54]. Thiol-based junctions tend to show broad conductance features owing to the large variability in the anchor–electrode contact geometry. Several groups have studied the effect of binding geometry on conductance[55–59], but understanding and thus gaining control over the variability of contact geometry is an ongoing challenge in the field[42,60–62].

Au–C contacts are particularly promising covalent anchors because they give well-defined conductance peaks owing to the selective binding to undercoordinated gold[63]. Furthermore, molecular wires with Au–C contacts generally demonstrate higher conductance peak values than structurally analogous wires with Au–S contacts. For example, the Au–benzenedithiol–Au junction shows a broad conductance, with reported conductance peak values ranging from 10^{-2} to 10^{-4} G_0 (REFS 11,64–66). By contrast, the structurally similar Au–xylyl–Au junction conducts at 0.9 G_0 (REF. 67). The difference in conductance arises from two factors. First,

the C–Au bond is more strongly coupled to the π system than the S–Au bond because it is much shorter in bond length. Second, ΔE is much smaller for the Au–C gateway states that describe the covalent metal–molecule hybridization. For example, the Au–S gateway state is centred at $E - E_F = -1.4$ eV for alkane dithiols[59], whereas the Au–C gateway state is centred at $E - E_F = -0.8$ eV for bis(trimethylstannyl)alkanes[67]. This difference in energy alignment with the E_F contributes significantly to the difference in conductance.

Three methods have been developed for the *in situ* generation of direct Au–C covalent contacts. The first method involves the transmetalation of C–SnR_3 bonds on gold surfaces to generate C–Au bonds (and tin oxide by-products under ambient conditions[68]). This method was first used to obtain self-assembled alkane monolayers on gold surfaces from organotin species[69], and it was later used for the *in situ* cleavage of terminal C–$SnMe_3$ bonds to obtain covalent Au–arene and Au–alkane contacts in single-molecule junctions[67]. Alkane[67] and paraphenylene[70] wires terminated with Au–CH_2R contacts demonstrate a 10- to 100-fold increase in conductance compared with the analogous bridges terminated with dative Au–NH_2R contacts. The applicability of this method was recently expanded to include Au–acetylene contacts[71]. A potential shortcoming of this approach is that it both uses and produces toxic and volatile trimethyltin species. Furthermore, this reaction does not occur universally for all organotin molecules; for example, this manner of cleavage does not occur in perfluorinated benzene backbones[70]. The most important molecular design rule for creating C–Au contacts via C–SnR_3 transmetallation on gold is that the bond between the molecular bridge and the tin atom must be the most reactive of the four organotin bonds. For example, *n*-alkane backbones with $SnBu_3$ end groups do not show clean conductance features in the STM break junction[67], presumably because the cleavage of the four C–Sn bonds is not selective. By contrast, Au–$(CH_2)_n$–Au junctions form cleanly for trimethyltin-terminated alkane wires because of the greater stability of $RH_2C^{\bullet}$ radicals compared with $H_3C^{\bullet}$, which enables the preferential cleavage of the RH_2C–Sn bond. Similarly, benzyltrimethyltin molecules cleave instantaneously at the Sn–benzyl bond, even at −110 °C (REF. 63), whereas Sn–aryl bonds cleave slowly, with Au–aryl–Au junctions appearing only after 2.5 hours at room temperature[67]. This design strategy allows the programming of the junction that will form on Sn–C cleavage.

The second method for obtaining covalent Au–C contacts involves a fluoride-initiated desilylation of oligo(phenylene ethynylene) wires terminated with trimethylsilyl (TMS) end groups[72]. Addition of tetrabutylammonium fluoride to a solution of the TMS-protected target molecules selectively cleaves the terminal ethynyl–Si bonds. This approach is inspired from a classic synthetic chemistry method that exploits the strong affinity between silicon and fluorine to unmask acetylene groups[73]. The applicability of this method is hindered by the NBu_4^+ electrolytes that participate in ionic conductance between the electrodes; these electrolytes give rise to significant conductance noise that may cover the signal of low-conductance molecules. However, ionic conductance can be reduced by coating the electrodes with an insulating layer[74].

The third method to produce covalent electrode anchors involves the electroreduction of diazonium salts on gold surfaces[75]. It was first used in the context of break-junction experiments by electrochemically reducing the terminal diazonium end groups on a biphenyl ring to generate covalent Au–biphenyl–Au junctions[76]. This approach is attractive because covalent Au–C contacts can be generated on demand by increasing the reduction potential via a gate electrode to irreversibly cleave the aryl–N bond. However, diazonium salts are known to be thermally unstable and, in many cases, explosive[77]. In particular, alkyl diazonium salts are especially unstable, which limits the range of diazonium-functionalized structures that can be easily measured in single-molecule junctions.

There are still many unsolved issues in the implementation of single-molecule devices with covalent contacts. The choice of precursors for the desilylation and diazonium reduction methods has been limited thus far to those that place the Au–C bonds in the σ plane of the molecular bridge. This is an important consideration because maintaining coplanarity between the metal–carbon bond and the bridge π system is essential for optimizing the coupling between molecule and electrode. Moreover, molecular wires with Au–C contacts are not particularly robust, as they tend to oligomerize *in situ* during break-junction experiments. This may be unavoidable under ambient conditions, as Au–C bonds are inherently sensitive to oxidation and dimerization pathways. Tuning the structure of the wire to make the metal–carbon bond more stable is a possible solution to avoid device failure. Using electrode materials that form more stable electrode–carbon bonds is another possible route for enhancing the stability of the device; we discuss this topic in the following section.

Electrode

The electrode as a chemical reagent. Using the electrode as a reagent in synthetic reactions is a promising and underexplored route for the development of SME devices with desirable properties. Concepts in organometallic chemistry describe how the electronic structure of different metals affects their chemical reactivity. Inorganic chemical principles, such as the hard–soft acid–base concept and ligand field theory, provide a general roadmap for understanding the chemical groups that can be used to functionalize electrode surfaces; 'soft' metals that are commonly used as electrode materials interact strongly with 'soft' and high-field ligands[32,78], such as the ones depicted in FIG. 2a. Several classic organometallic and organic reactions have already been transposed from reaction flasks to electrode surfaces. For example, the Ullmann coupling reaction, which uses the metal-mediated homocoupling of halobenzenes to fuse aryl rings together, was discovered[79] in 1901 — more than a century later it was reimagined on a gold surface to synthesize graphene

nanoribbons[80,81]. The coupling reactions between an amine and a carboxylic acid, which are fundamental for peptide chemistry, have been used to produce covalent electrode–molecule–electrode junctions by reacting amine-terminated molecules with carboxylate point defects in carbon-nanotube electrodes[18]. The ruthenium alkylidene chemistry familiar to olefin metathesis reactions[82] has been used for functionalizing ruthenium electrodes with alkylidenes that are well coupled, which is relevant for charge transport, and catalytically active, so that longer wires can be grown[83]. As the field of SMEs develops, more examples will arise in which the reactivity profile of specific metals is exploited to functionalize electrode surfaces.

Electrode materials. Gold is the most common electrode material in break-junction experiments because of its inertness, which enables the measurement of single-molecule junctions with consistency and reproducibility under ambient conditions. Other metals have interesting electronic properties, but many of them quickly oxidize in air, creating oxide layers on the electrode surface that prevent the clean formation of metal–molecule–metal junctions. Measuring in air-free or ultrahigh vacuum conditions can help to circumvent this problem but adds a significant degree of complexity to the experiment. Electrode materials that have been used for SME devices include metals such as Ag[84,85], Pd[86] and Pt[87–89], and graphitic nanostructures such as graphene[19] and carbon nanotubes[18].

The density of states of a metal at the E_F strongly influences the conductance of the single-molecule junction. This was demonstrated in a study on isothiocyanate-terminated alkanes, in which the observed conductance was two- to threefold higher in Pd and Pt junctions than in Au junctions[90]. The metal *d* band possesses the appropriate symmetry to couple with the isothiocyanate π orbitals near the E_F; thus, the increased *d* character at the E_F of Pd and Pt relative to Au enhances the metal–molecule d–π interaction[91]. In another study, it was found that the conductance peak value in 4,4′-bipyridine is more than an order of magnitude lower when it is measured with Ag electrodes rather than Au electrodes. This difference in conductance arises from the weaker d_{yz}-orbital character of the Ag density of states at the E_F that results in reduced d–π^* hybridization and metal–molecule coupling[92] (FIG. 3c). Metals with unpaired spins can also confer interesting magnetic properties to single-molecule junctions[93–95]. Harnessing the unique chemical and physical properties of different electrode materials will allow a greater degree of control over charge transport in single-molecule junctions and will enable the design of new SME devices.

Molecular bridge

The idea that a molecule can function as an active component in an electrical circuit was first formulated in the context of the design of a theoretical rectifier with an asymmetric molecular bridge structure, in which charge would flow preferentially from electron-rich to electron-deficient regions[1]. Out of the three modules of the molecular junction, the bridge has the greatest potential for manipulation with synthetic chemistry: any chemically reasonable structure can be prepared and can serve as a molecular bridge as long as it contains two anchoring groups. There are two distinct subcomponents in the bridge: the backbone and the substituents. The backbone is the main pathway through which charge flows — such as the π bonds in phenyl rings or the Si–Si σ bonds in oligosilanes. The substituents are the chemical groups attached to the main backbone chain, and they can alter both the electronic structure and the conformation of the molecule.

β values and electronic coupling in the molecular backbone. The ability of different oligomeric backbones to transport charge can be evaluated by comparing how their conductance decays with increasing oligomer length. This is quantitatively described by their β values, which are given in units of inverse length. The β value is derived by plotting conductance on a semi-logarithmic scale against the molecular length (L) of the oligomer. The β value is then extracted using the formula $G = Ae^{-\beta L}$. β values depend on the coupling strength between repeat units: backbones that are strongly conjugated and effective at transporting charge have a shallow conductance decay and, consequently, a low β value. Here, we limit the discussion to β values obtained from measurements of single molecules (rather than molecular assemblies), in which conductance is dominated by coherent tunnelling mechanisms. Excellent reviews have been written that discuss β values obtained from a wider range of measurement techniques, wire structures and conductance mechanisms[96,97].

Representative β values for several oligomeric materials that conduct via coherent tunnelling are listed in TABLE 1. Alkanes are characterized by high β values (0.84 $Å^{-1}$) because they do not have strongly conjugated bonds that can carry charge[12,57]. Permethyloligosilanes ($[SiMe_2]_n$) terminated with methylthiomethyl electrode linkers have a β value (0.39 $Å^{-1}$) comparable to that of aromatic π conductors[48]. Despite their structural similarity to alkanes, oligosilanes transport charge more effectively because Si–Si σ bonds are more strongly conjugated than C–C σ bonds, as their bonding orbitals are much larger in size and much higher in energy[98]. From the perspective of the transmission function (BOX 1), the nearest neighbour coupling τ in silanes is stronger than in alkanes. The low β value in silanes also opens up the possibility of observing QI effects in σ systems, as discussed further below. Isostructural permethyloligogermanes also have a low β value (0.36 $Å^{-1}$), which is slightly lower than that of permethyloligosilanes[49].

π-conjugated backbones tend to be associated with low β values. Conjugated but non-aromatic systems typically have a lower β value than purely aromatic species. Mapping the conductance of molecular wires against their degree of aromaticity suggests that the conductance is inversely proportional to the resonance stabilization energy[99]. In the transmission picture, this aromatic stabilization energy decreases the on-site energies (ε), thereby lowering ΔE (BOX 1). The higher

conductance of non-aromatic structures is supported by bulk-scale conductance[100] and optoelectronic[101] experiments, which show that polymer backbones with strong quinoidal character (and consequently weak aromatic character) are superior at delocalizing charge along the backbone. Anti-aromaticity describes the energetic destabilization that arises from the interaction of $(4n)$ π electrons in a planar ring. These destabilized structures should possess a high HOMO energy, and it has been predicted that anti-aromatic compounds will exhibit high conductance[102]. However, the instability of purely anti-aromatic structures has precluded their study in SMEs.

Substituent effects on conductance. Synthetic modification of the substituent structure is another handle for altering the charge-transport properties of the molecular wire. The relationship between substituent electronics and conductance was explored in 1,4-diaminobenzene-based molecular wires, in which different substituents were introduced at the 2-, 3-, 5- and 6- positions. It was determined that, in this particular system, electron-donating groups (such as –Me and –OMe) increase conductance, whereas electron-withdrawing groups (such as $-CF_3$, –Br, –Cl and –F) decrease conductance[103]. These trends arise from the HOMO-conducting nature of the amine linkers; substituents that push electron density into the benzene ring raise the HOMO energy towards the E_F of gold. Electron-withdrawing substituents stabilize the backbone and lower the HOMO energy away from the E_F. These findings can be analysed in the context of physical organic chemistry by constructing a Hammett plot from molecular conductance and the Hammett constants (σ_{para})[104] (FIG. 3d). Hammett constants were originally quantified to correlate the electron-withdrawing ($-\sigma_{para}$) or electron-donating ($+\sigma_{para}$) nature of *para*-linked aromatic substituents with chemical reactivity. This relationship between σ_{para} and conductance, demonstrated in FIG. 3d, suggests that, just as chemical reaction rates depend on the differences in energy between the ground state and the transition state, conductance is related to the energy difference between the metal–molecule hybridized conducting orbital and the E_F. The same general principle is observed in single-molecule thermoelectric devices based on benzene dithiol junctions, in which electron-donating substituents increase the Seebeck coefficient (hole-transporting character) and electron-withdrawing substituents decrease it[105].

Table 1 | **β values of oligomeric materials with conductance dominated by coherent-tunnelling mechanisms**

Backbone	Structure	β ($Å^{-1}$)	Refs
Alkane		0.84	57
Silane		0.39	48
Germane		0.36	49
Alkene		0.22	145
Alkyne		0.17–0.32	44
p-phenylene	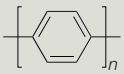	0.43	13
p-phenylene ethynylene	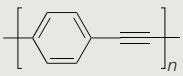	0.20, 0.34	146,147
Thiophene	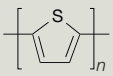	0.16, 0.4	138,148
Thiophene dioxide	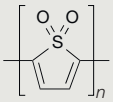	0.20	41
Cyclopenta-difluorene	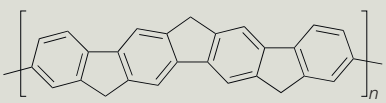	0.21	149

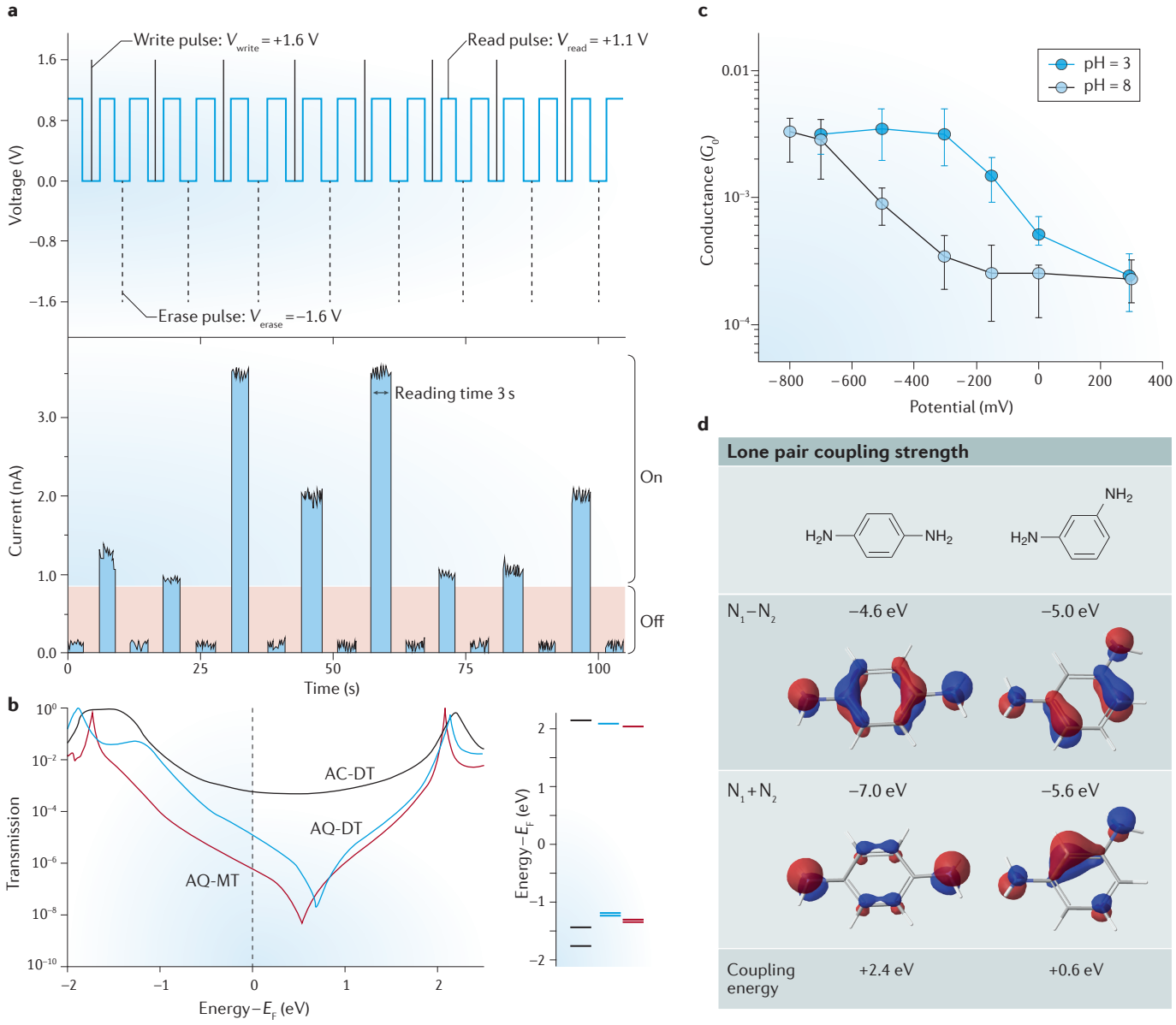

Figure 4 | **Single-molecule conductance switches and quantum interference features. a** | Reversible voltage-induced switching between on and off states in an oligo(phenylene ethynylene)-based wire. **b** | Calculated transmission for monothiolated anthraquinone (AQ-MT), dithiolated anthraquinone (AQ-DT) and dithiolated anthracene (AC-DT). The diagram on the right depicts the energy levels (from top to bottom) of the lowest unoccupied molecular orbital (LUMO), the highest occupied molecular orbital (HOMO) and the HOMO-1 of AC-DT, AQ-DT and AQ-MT. AQ-MT and AQ-DT exhibit anti-resonance features. **c** | The plotted points represent conductance peak values at particular gate potentials and pH values for an anthracene and anthraquinone-based quantum interference switch. **d** | Isosurfaces of the two highest occupied molecular orbitals containing lone pair character that exhibit anti-symmetric ($N_1 - N_2$) and symmetric ($N_1 + N_2$) lone pair phases (B3LYP/6-31G**). The difference in energy between these two states corresponds to the coupling strength between the two lone pairs. Molecules with strongly coupled lone pairs typically do not demonstrate anti-resonance quantum interference features near the Fermi level, E_F. Panel **a** is reproduced with permission from REF. 118, Wiley–VCH. Panel **b** is from REF. 123, Nature Publishing Group. Panel **c** is adapted with permission from REF. 125, Wiley–VCH.

Various research groups have studied the conformation–conductance relationship in biphenyl rings by synthetically modifying the 2,2′ substituents to alter the torsion angle between the two phenyl rings[13,106,107]. Regardless of whether the biphenyl rings are terminated by π- or π^*-conducting anchors, conductance decreases as the torsion angle (φ) increases and the conjugation between the rings weakens (FIG. 3e). In reference to the transmission picture described in BOX 1, the τ coupling between neighbouring sites decreases with $\cos(\varphi)$. These examples illustrate how synthetic variations of the substituent group can alter conductance by tuning the electronics or stereochemistry of the molecular backbone.

Emerging areas in single-molecule electronics

In the previous section, we explored how altering the molecular wire structure and stereochemistry can affect the fundamental charge-transport properties of the single-molecule junction. In this section, we discuss how the structural units of the junction (particularly the anchor and the bridge) can be manipulated to create new SME devices. Many sophisticated switching platforms made of ensembles of molecules have been developed and are thoroughly discussed in other reviews[5,96,108,109]; here, we focus specifically on the opportunities and challenges in the development of single-molecule devices that switch conductance reversibly and on demand between stable on–off states. We then discuss how QI, an emerging phenomenon specific to molecular-scale devices, depends on the strength of electronic communication between the anchor groups through the bridge. We conclude by rationalizing QI from a chemical perspective.

Incorporating switching functions into the junction. There are many examples of multimodal switching from solution-phase chemistry, in which the molecule can switch between different isomers using optical, electrochemical or pH triggers. However, the ability of a molecule to switch in solution is not always retained when it is bound to electrodes. First, the activation barrier for switching needs to be high enough so that the switching can be induced predictably and will not occur randomly. For example, it was demonstrated in a bianthrone-based device that even if the barrier between bistable states is high for the free molecule in solution, the barrier between these states can lower as the molecular orbitals hybridize with the orbitals of the electrode and cause switching to occur uncontrollably even at low temperatures[110].

Second, holding the molecule at a fixed distance between two electrodes can prevent switching in systems in which the two states have different anchor-to-anchor lengths. For this reason, there are many studies on switching between *cis* and *trans* isomers in stilbene and azobenzene ensembles in which the molecules only need to be bound at one electrode; however, controlled switching between *cis* and *trans* isomers in a single metal–molecule–metal junction has yet to be reported.

Last, and more specific to photoswitching, if the coupling between the electrode and a photoactive molecule is strong, the photoexcited state of the molecule can transfer charge to the electrode rather than photoisomerizing. This mechanism is thought to be the reason why certain diarylethene switches, despite having on- and off-state geometries of similar molecular length, do not operate reversibly in break-junction setups[111]. Such problems can potentially be circumvented by synthesizing wire structures in which the backbone is decoupled from the electrode[112].

It is challenging to create a system in which switching occurs in a single metal–molecule–metal junction. Although many examples of switching triggered by pH[113,114] and light[112,115] have been reported, they typically do not describe switching within the same individual molecule. Mechanically triggered switching[22,25,48], in which the stretching or compressing of the junction induces the switching, and voltage-triggered switching[116–118] (FIG. 4a) have been used to successfully switch conductance in individual junctions. However, this approach is difficult to implement in devices in which the electrodes must be stationary or the voltage bias between two terminals must be held constant. There is much potential for growth in this branch of SMEs; innovations in synthesis and engineering will promote the development of single-junction conductance switches, which are crucial for the realization of single-molecule logic and memory components.

Quantum interference effects. The concept of QI was first developed to describe the wave interference of photons and electrons in the context of double-slit experiments. In the SMEs community, the term 'quantum interference' has been appropriated to describe the interference between the electron waves propagating through molecular orbitals in a single-molecule junction[119–121]. QI-based devices have captured the imagination of many in the SMEs community because there are no parallels in conventional solid-state electronics. Constructive interference enhances conductance, whereas destructive interference suppresses conductance. Constructive QI has been reported in a double-backbone junction, in which the observed conductance was found to exceed the conductance of two single-backbone junctions operated in parallel[122]. The SMEs field has focused its attention mostly on destructive QI, which is characterized by a sharp dip or an 'anti-resonance' in the transmission probability of non-equilibrium Green's function calculations (FIG. 4b) or in differential conductance experiments[123,124]. These anti-resonances are most relevant for single-molecule conductance when they occur near the electrode E_F (but can occur anywhere in the energy landscape).

When destructive interference occurs near the E_F of the electrode, little or no conductance is observed. This is appealing because the destructive QI pathway, if it can be switched on demand, might serve as an off state that is exceedingly low in conductance; thus, QI offers a potential route for the creation of molecular devices with large on/off ratios. Many theoretical devices[119,120] of this kind have been imagined, in which the device can either gate the position of the anti-resonance or switch the transport pathway through the molecule between non-QI and destructive-QI pathways — however, few of these devices have been experimentally realized. Recently, several groups have created QI switches in which electrochemical triggers induce bulk switching between cross-conjugated anthraquinone (QI) and linearly conjugated dihydroxyanthracene (non-QI) backbone structures that differ in conductance by more than an order of magnitude[125,126] (FIG. 4c).

The notion of destructive QI is quite familiar to chemists, although from a different perspective. For example, *para*-substituted phenyl rings yield high

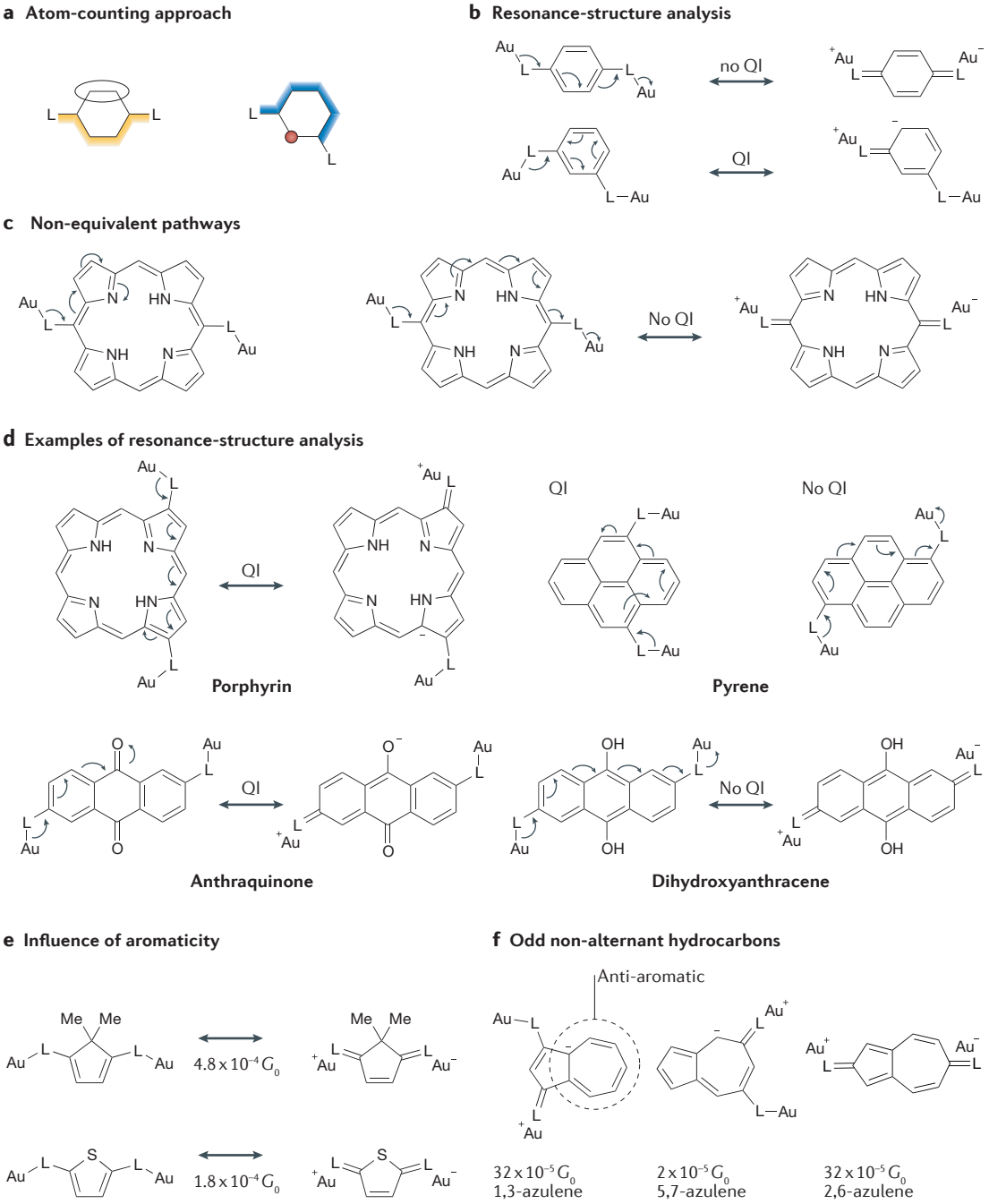

Figure 5 | **Pen-and-paper methods to predict quantum interference. a** | In the atom-counting approach, a continuous path is drawn from one linker to the other. A circle is drawn around neighbouring-atom pairs that are off path, as in the *para* case. If there are single atoms that are off path and do not have an off-path neighbour, as in the *meta* case, destructive quantum interference (QI) is expected to occur. **b** | Resonance-structure analysis to predict QI. **c** | When there are two non-equivalent pathways, as in the pyrrole ring, some arrow-pushing pathways are 'dead ends' (left panel). A good pathway is also shown (right panel). **d** | Resonance-structure analysis of QI in porphyrin, pyrene, anthraquinone and dihydroxyanthracene. **e** | Conductance peak values and resonance structures for 2,5-disubstituted cyclopentadiene (top panel) and thiophene (bottom panel). The conductive quinoidal resonance form makes a more important contribution to the electronic structure of the cyclopentadiene compared with that of the thiophene because the former is non-aromatic. **f** | Conductance peak values and resonance structures of azulene constitutional isomers. Both 1,3-azulene and 5,7-azulene isomers show strong anti-resonances in their calculated transmission functions, but the anti-resonance is shifted towards a higher energy for 1,3-azulene — its transmission is then much higher at the Fermi level, E_F. The 1,3-azulene isomer demonstrates an anti-aromatic resonance structure, whereas the 5,7-azulene isomer does not. The 2,6-isomer is as conductive as the 1,3-isomer, even though it does not have a QI feature near the E_F.

conductance values, whereas *meta*-substituted phenyl rings demonstrate substantially attenuated conductance owing to destructive interference pathways[40,127]. This destructive QI ultimately arises from the node at the *meta* position in the HOMO that prevents electronic coupling between two *meta* substituents. Therefore, *meta*-linked wires show poor conductance and destructive QI for the same reason that electrophilic aromatic substitution reactions with electron-rich substituents, in general, do not occur at the *meta*-position. Cross-conjugated structures, such as the anthraquinone molecule in the example above, often show anti-resonances in their transmission probability calculations[128] for essentially the same reason — the two primary unsaturated pathways are not conjugated with each other. The lack of communication between the two unsaturated ends of a cross-conjugated molecule has been well established in the context of chemical reactivity and spectroscopy[129].

The coupling strength between the two anchor groups through the bridge is thus strongly related to QI and conductance. This coupling strength can be qualitatively evaluated from ground-state density functional theory computations that model the electronic structure of the molecule, as shown in FIG. 4d for 1,3- and 1,4-diaminobenzene. Our analysis is limited to the two highest occupied molecular orbitals that contain the lone pair orbitals. The phases of the two lone pairs (N_1 and N_2) are typically symmetric in one of these molecular orbitals ($N_1 + N_2$) and anti-symmetric in the other ($N_1 - N_2$). The energy needed to decouple the lone pairs can be estimated by considering the energy cost of adding or subtracting these molecular orbitals from each other, which would localize the orbital density on N_1 or N_2, respectively. The energy difference between these two molecular orbitals is 2.4 eV for 1,4-diaminobenzene and 0.6 eV for 1,3-diaminobenzene; therefore, coupling is significantly stronger in the *para*-linked molecule than in the *meta*-linked molecule. This analysis can be extended to other simple aromatic systems to rationalize conductivity trends that arise from varying linker connectivity or backbone composition[130].

Several other methods have been developed to predict QI in alternant π-conjugated systems. With 'orbital symmetry rules', it is possible to predict whether QI occurs in naphthalene systems with different linker connectivity points[131]. The orbital-symmetry approach is based on a qualitative comparison of the phases of the ring carbon orbitals in the HOMO and in the LUMO. This methodology was also used to elucidate the relationship between switching ratio and anchor-group connectivity in photoactive molecules[132].

'Pen-and-paper' methods for predicting quantum interference. Simple graphical methods, such as the star labelling formalisms of orbital pairing in molecular orbital theory[133], can be used to predict whether even-alternant hydrocarbons demonstrate 'alike' (QI) or 'disjoint' (non-QI) coupling[128]. 'Atom-counting' approaches can also be used to forecast destructive QI in cyclic and acyclic π-conjugated molecules[134] (FIG. 5a). These graphical approaches are useful because only a pen and paper is required to quickly predict whether there is QI in a molecular structure. These methods should be familiar to reaction chemists because they are essentially shorthand for arrow pushing in π-conjugated resonance forms. It is then reasonable that QI can be predicted by simply drawing and analysing resonance structures.

Resonance structures are simple representations of the π-electron interactions in conjugated molecules. No single resonance structure is entirely descriptive of the electronic character of a π-conjugated molecule, and the molecule does not interconvert between resonance structures — rather, the electronic structure is a weighted average of resonance forms. The rules and conventions for drawing reasonable resonance structures by arrow pushing can be found in any introductory organic chemistry textbook. 'Resonance logic' can be used to predict QI in π-conjugated molecules (FIG. 5b) by the following steps. First, draw the chemical structure of the molecular bridge with Au atoms attached to each linker (L) atom. Second, attempt to draw a reasonable resonance structure that delocalizes one L–Au bond onto the other Au atom by using arrow-pushing formalisms. If it is possible to draw a resonance structure where there is a quinoidal structure in the molecular bridge, a positive charge on one Au atom and a negative charge on the other Au atom, QI should not occur. If there are non-equivalent pathways in an aromatic ring, the choice of pathway is important, because some pathways do not connect the Au atoms (FIG. 5c). All pathways must be sampled before determining whether there is QI in the structure. The reasonable range of resonance structures used in this approach is limited to those that possess a single positive and a single negative charge. This ensures that only the fate of the original L–Au bond is tracked. Last, if there are no resonance structures that can be drawn that meet the criteria in the second step, the molecule should demonstrate destructive QI.

According to these rules, QI essentially depends on whether it is possible to draw a resonance structure of the junction in which one linker–electrode bond delocalizes through the π-conjugated bridge onto the other electrode atom. This is reasonable because conductance describes how well one electrode is connected with the other through the conjugated molecule. The charges that are drawn on the Au atoms in non-QI resonance structures are symbolic of charge transfer between the electrodes. If there is no resonance form that connects the Au electrodes in a single path through the π system, destructive QI occurs. FIGURE 5d shows that this approach holds for various π systems such as porphyrins[135,136], pyrenes[137], anthraquinones[123] and anthracenes[123]. For practice, readers can try this method on various other polycyclic aromatic hydrocarbons and check the answers against the corresponding transmission calculations[138].

The resonance-structure approach is valuable because it is compatible with chemical intuition. It can

be used not only to predict QI but also to explain why aromaticity tends to diminish charge-transport ability. FIGURE 5e depicts the aromatic and quinoidal resonance structures of 2,5-disubstituted cyclopentadiene and thiophene[99]. The quinoidal resonance form optimizes coupling between the electrodes, as stipulated by the resonance-structure analysis above. However, aromatic wires have weak quinoidal character because of the strong stabilizing energy associated with aromaticity. Conductance is thus higher for nonaromatic wires because their electronic structures are more quinoidal in character.

In odd non-alternant hydrocarbons, such as azulene, QI pathways can still result in strong conductance[46]. The 1,3- and 5,7-disubstituted azulene isomers both demonstrate transmission anti-resonances, but the 1,3-isomer gives a much higher conductance (FIG. 5f) owing to the shift of its anti-resonance position towards a higher energy. The 1,3-isomer is as conductive as the 2,6-isomer that does not have a QI feature near the E_F. If we draw the reasonable resonance structures for the 1,3- and 5,7-isomers, it becomes immediately clear that the 1,3-isomer has an anti-aromatic resonance form, whereas the 5,7-isomer does not. Recalling that anti-aromaticity is expected to result in enhanced conductance, it can be understood why the 1,3-isomer has the higher conductance despite the poor coupling between the anchor groups through the conductive π pathway.

Despite the speed and the ease of these pen-and-paper approaches, there are also limitations. They cannot be used to quantitatively predict the conductance value or the position of the anti-resonance peak in transmission calculations. Furthermore, they can only be used to predict QI in π-conducting systems; simple methods for predicting QI in σ-conjugated systems, such as silanes, do not yet exist. More sophisticated methods must be used in these instances[139]. However, these simple methods are powerful because they enable rapid prediction of whether a molecular structure will exhibit QI. They can be used to quickly draw the resonance structures of many complex π-conjugated structures and to rapidly screen which of these compounds might possess interesting or anomalous QI properties.

Perspectives

In all realms of science, great progress can be made when lessons from the past are applied to understand the challenges and opportunities of the present and future. The ideas at the base of the emerging field of SMEs are rooted in the same principles developed in chemistry over the past century. In this Review, we have discussed the benefits and opportunities that arise from using chemical principles to guide the design and understanding of functional molecular electronic components.

Concepts borrowed from reaction chemistry continue to inspire new SME devices — but, at the same time, discoveries in SMEs produce new knowledge in chemistry, engineering and other fields of science. Research in SMEs, particularly through scanning probe measurements on self-assembled monolayers, has shed light on how molecules assemble and behave when adsorbed or bonded to metal surfaces[53,140]. Extrapolating molecular conductance from these densely packed monolayer assemblies provides information on how molecules communicate with one another and with their surroundings in thin molecular films[52]. Single-molecule QI concepts have recently been used to design new ligand dyes for dye-sensitized solar cells and new dielectric materials[141,142]. The discoveries made in the context of SMEs are also relevant for current and future integrated circuit technologies. The insights gained from studying conductance at the molecular scale will help us to understand how the charge-transport properties of semiconducting materials might change as their dimensions decrease and they begin to resemble molecules rather than bulk solids.

The past two decades have seen a vast deepening in the knowledge of how to create, measure and understand single-molecule junctions. One of the immediate challenges is how to use this newly gained knowledge to incorporate these structures into system-level devices. These new nanoscale architectures and interconnections could revolutionize nanoscale electronics by providing access to the vast store of structures available through synthetic chemistry. The combination of synthetic chemistry and electronics is an inspiration for the creation of fields and applications yet to be imagined.

1. Aviram, A. & Ratner, M. A. Molecular rectifiers. *Chem. Phys. Lett.* **29**, 277–283 (1974).
2. Choi, H. & Mody, C. C. M. The long history of molecular electronics: microelectronics origins of nanotechnology. *Soc. Stud. Sci.* **39**, 11–50 (2009).
3. Tao, N. J. Electron transport in molecular junctions. *Nat. Nanotechnol.* **1**, 173–181 (2006).
4. Moth-Poulsen, K. & Bjørnholm, T. Molecular electronics with single molecules in solid-state devices. *Nat. Nanotechnol.* **4**, 551–556 (2009).
5. Aradhya, S. V. & Venkataraman, L. Single-molecule junctions beyond electronic transport. *Nat. Nanotechnol.* **8**, 399–410 (2013).
6. Ward, D. R., Scott, G. D., Keane, Z. K., Halas, N. J. & Natelson, D. Electronic and optical properties of electromigrated molecular junctions. *J. Phys. Condens. Matter* **20**, 374118 (2008).
7. Bumm, L. A. *et al.* Are single molecular wires conducting? *Science* **271**, 1705–1707 (1996).
8. Moreland, J. & Ekin, J. W. Electron tunneling experiments using Nb–Sn 'break' junctions. *J. Appl. Phys.* **58**, 3888–3895 (1985).
9. Muller, C. J., van Ruitenbeek, J. M. & de Jongh, L. J. Experimental observation of the transition from weak link to tunnel junction. *Phys. C Supercond.* **191**, 485–504 (1992).
10. Smit, R. H. M. *et al.* Measurement of the conductance of a hydrogen molecule. *Nature* **419**, 906–909 (2002).
11. Reed, M. A. Conductance of a molecular junction. *Science* **278**, 252–254 (1997).
12. Xu, B. & Tao, N. J. Measurement of single-molecule resistance by repeated formation of molecular junctions. *Science* **301**, 1221–1223 (2003).
13. Venkataraman, L., Klare, J. E., Nuckolls, C., Hybertsen, M. S. & Steigerwald, M. L. Dependence of single-molecule junction conductance on molecular conformation. *Nature* **442**, 904–907 (2006).
14. Wold, D. J. & Frisbie, C. D. Formation of metal–molecule–metal tunnel junctions: microcontacts to alkanethiol monolayers with a conducting AFM tip. *J. Am. Chem. Soc.* **122**, 2970–2971 (2000).
15. Park, H., Lim, A. K. L., Alivisatos, A. P., Park, J. & McEuen, P. L. Fabrication of metallic electrodes with nanometer separation by electromigration. *Appl. Phys. Lett.* **75**, 301–303 (1999).
16. Andres, R. P. *et al.* Self-assembly of a two-dimensional superlattice of molecularly linked metal clusters. *Science* **273**, 1690–1693 (1996).
17. Cui, X. D. *et al.* Reproducible measurement of single-molecule conductivity. *Science* **294**, 571–574 (2001).
18. Guo, X. *et al.* Covalently bridging gaps in single-walled carbon nanotubes with conducting molecules. *Science* **311**, 356–359 (2006).
19. Prins, F. *et al.* Room-temperature gating of molecular junctions using few-layer graphene nanogap electrodes. *Nano Lett.* **11**, 4607–4611 (2011).

20. Morpurgo, A. F., Marcus, C. M. & Robinson, D. B. Controlled fabrication of metallic electrodes with atomic separation. *Appl. Phys. Lett.* **74**, 2084–2086 (1999).
21. Chen, X. *et al.* Chemical fabrication of heterometallic nanogaps for molecular transport junctions. *Nano Lett.* **9**, 3974–3979 (2009).
22. Quek, S. Y. *et al.* Mechanically controlled binary conductance switching of a single-molecule junction. *Nat. Nanotechnol.* **4**, 230–234 (2009).
23. Su, T. A. *et al.* Silicon ring strain creates high-conductance pathways in single-molecule circuits. *J. Am. Chem. Soc.* **135**, 18331–18334 (2013).
24. Kiguchi, M. *et al.* Single molecular resistive switch obtained via sliding multiple anchoring points and varying effective wire length. *J. Am. Chem. Soc.* **136**, 7327–7332 (2014).
25. Moreno-García, P. *et al.* Charge transport in C_{60}-based dumbbell-type molecules: mechanically induced switching between two distinct conductance states. *J. Am. Chem. Soc.* **137**, 2318–2327 (2015).
26. Lafferentz, L. *et al.* Conductance of a single conjugated polymer as a continuous function of its length. *Science* **323**, 1193–1197 (2009).
27. Meisner, J. S. *et al.* A single-molecule potentiometer. *Nano Lett.* **11**, 1575–1579 (2011).
28. Leary, E. *et al.* Unambiguous one-molecule conductance measurements under ambient conditions. *Nano Lett.* **11**, 2236–2241 (2011).
29. Martin, C. A. *et al.* Fullerene-based anchoring groups for molecular electronics. *J. Am. Chem. Soc.* **130**, 13198–13199 (2008).
30. Aradhya, S. V., Frei, M., Hybertsen, M. S. & Venkataraman, L. Van der Waals interactions at metal/organic interfaces at the single-molecule level. *Nat. Mater.* **11**, 872–876 (2012).
31. Heimel, G. *et al.* Charged and metallic molecular monolayers through surface-induced aromatic stabilization. *Nat. Chem.* **5**, 187–194 (2013).
32. Schläfer, H. L. & Gliemann, G. *Basic Principles of Ligand Field Theory* (Wiley-Interscience, 1969).
33. Venkataraman, L. *et al.* Single-molecule circuits with well-defined molecular conductance. *Nano Lett.* **6**, 458–462 (2006).
34. Reddy, P., Jang, S.-Y., Segalman, R. A. & Majumdar, A. Thermoelectricity in molecular junctions. *Science* **315**, 1568–1571 (2007).
35. Widawsky, J. R., Darancet, P., Neaton, J. B. & Venkataraman, L. Simultaneous determination of conductance and thermopower of single molecule junctions. *Nano Lett.* **12**, 354–358 (2012).
36. Derosa, P. A. & Seminario, J. M. Electron transport through single molecules: scattering treatment using density functional and green function theories. *J. Phys. Chem. B* **105**, 471–481 (2001).
37. Kamenetska, M. *et al.* Conductance and geometry of pyridine-linked single-molecule junctions. *J. Am. Chem. Soc.* **132**, 6817–6821 (2010).
38. Lee, W. *et al.* Heat dissipation in atomic-scale junctions. *Nature* **498**, 209–212 (2013).
39. Koga, J., Tsuji, Y. & Yoshizawa, K. Orbital control of single-molecule conductance perturbed by π-accepting anchor groups: cyanide and isocyanide. *J. Phys. Chem. C* **116**, 20607–20616 (2012).
40. Mayor, M. *et al.* Electric current through a molecular rod — relevance of the position of the anchor groups. *Angew. Chem. Int. Ed. Engl.* **42**, 5834–5838 (2003).
41. Dell, E. J., Capozzi, B., Xia, J., Venkataraman, L. & Campos, L. M. Molecular length dictates the nature of charge carriers in single-molecule junctions of oxidized oligothiophenes. *Nat. Chem.* **7**, 209–214 (2015).
42. Li, Z., Smeu, M., Ratner, M. A. & Borguet, E. Effect of anchoring groups on single molecule charge transport through porphyrins. *J. Phys. Chem. C* **117**, 14890–14898 (2013).
43. Park, Y. S. *et al.* Frustrated rotations in single-molecule junctions. *J. Am. Chem. Soc.* **131**, 10820–10821 (2009).
44. Moreno-García, P. *et al.* Single-molecule conductance of functionalized oligoynes: length dependence and junction evolution. *J. Am. Chem. Soc.* **135**, 12228–12240 (2013).
45. Batra, A. *et al.* Tuning rectification in single-molecular diodes. *Nano Lett.* **13**, 6233–6237 (2013).
46. Xia, J. *et al.* Breakdown of interference rules in azulene, a nonalternant hydrocarbon. *Nano Lett.* **14**, 2941–2945 (2014).
47. Danilov, A. *et al.* Electronic transport in single molecule junctions: control of the molecule–electrode coupling through intramolecular tunneling barriers. *Nano Lett.* **8**, 1–5 (2008).
48. Su, T. A., Li, H., Steigerwald, M. L., Venkataraman, L. & Nuckolls, C. Stereoelectronic switching in single-molecule junctions. *Nat. Chem.* **7**, 215–220 (2015).
49. Su, T. A. *et al.* Single-molecule conductance in atomically precise germanium wires. *J. Am. Chem. Soc.* **137**, 12400–12405 (2015).
50. Arroyo, C. R. *et al.* Influence of binding groups on molecular junction formation. *J. Am. Chem. Soc.* **133**, 14313–14319 (2011).
51. Li, H. *et al.* Electric field breakdown in single molecule junctions. *J. Am. Chem. Soc.* **137**, 5028–5033 (2015).
52. Tour, J. M. *et al.* Self-assembled monolayers and multilayers of conjugated thiols, α,ω-dithiols, and thioacetyl-containing adsorbates. Understanding attachments between potential molecular wires and gold surfaces. *J. Am. Chem. Soc.* **117**, 9529–9534 (1995).
53. Häkkinen, H. The gold–sulfur interface at the nanoscale. *Nat. Chem.* **4**, 443–455 (2012).
54. González, M. T. *et al.* Break-junction experiments on acetyl-protected conjugated dithiols under different environmental conditions. *J. Phys. Chem. C* **115**, 17973–17978 (2011).
55. Haiss, W. *et al.* Precision control of single-molecule electrical junctions. *Nat. Mater.* **5**, 995–1002 (2006).
56. Haiss, W. *et al.* Impact of junction formation method and surface roughness on single molecule conductance. *J. Phys. Chem. C* **113**, 5823–5833 (2009).
57. Li, X. *et al.* Conductance of single alkanedithiols: conduction mechanism and effect of molecule–electrode contacts. *J. Am. Chem. Soc.* **128**, 2135–2141 (2006).
58. Chen, F., Li, X., Hihath, J., Huang, Z. & Tao, N. Effect of anchoring groups on single-molecule conductance: comparative study of thiol-, amine-, and carboxylic-acid-terminated molecules. *J. Am. Chem. Soc.* **128**, 15874–15881 (2006).
59. Li, C. *et al.* Charge transport in single Au/alkanedithiol/Au junctions: coordination geometries and conformational degrees of freedom. *J. Am. Chem. Soc.* **130**, 318–326 (2008).
60. Inkpen, M. S. *et al.* New insights into single-molecule junctions using a robust, unsupervised approach to data collection and analysis. *J. Am. Chem. Soc.* **137**, 9971–9981 (2015).
61. Rascón-Ramos, H., Artés, J. M., Li, Y. & Hihath, J. Binding configurations and intramolecular strain in single-molecule devices. *Nat. Mater.* **14**, 517–522 (2015).
62. Li, Z. *et al.* Hapticity-dependent charge transport through carbodithioate-terminated [5,15-bis(phenylethynyl)porphinato]zinc(II) complexes in metal–molecule–metal junctions. *Nano Lett.* **14**, 5493–5499 (2014).
63. Batra, A. *et al.* Trimethyltin-mediated covalent gold–carbon bond formation. *J. Am. Chem. Soc.* **136**, 12556–12559 (2014).
64. Kim, Y., Pietsch, T., Erbe, A., Belzig, W. & Scheer, E. Benzenedithiol: a broad-range single-channel molecular conductor. *Nano Lett.* **11**, 3734–3738 (2011).
65. Ulrich, J. *et al.* Variability of conductance in molecular junctions. *J. Phys. Chem. B* **110**, 2462–2466 (2006).
66. Xiao, X., Xu, B. & Tao, J. Measurement of single molecule conductance: benzenedithiol and benzenedimethanedithiol. *Nano Lett.* **4**, 267–271 (2004).
67. Cheng, Z.-L. *et al. In situ* formation of highly conducting covalent Au–C contacts for single-molecule junctions. *Nat. Nanotechnol.* **6**, 353–357 (2011).
68. Kaletová, E. *et al.* The scope of direct alkylation of gold surface with solutions of C_1–C_4 *n*-alkylstannanes. *J. Am. Chem. Soc.* **137**, 12086–12099 (2015).
69. Khobragade, D. *et al.* Preparation of covalent long-chain trialkylstannyl and trialkylsilyl salts and an examination of their adsorption on gold. *Langmuir* **26**, 8483–8490 (2010).
70. Chen, W. *et al.* Highly conducting π-conjugated molecular junctions covalently bonded to gold electrodes. *J. Am. Chem. Soc.* **133**, 17160–17163 (2011).
71. Schwarz, F. *et al.* High-conductive organometallic molecular wires with delocalized electron systems strongly coupled to metal electrodes. *Nano Lett.* **14**, 5932–5940 (2014).
72. Hong, W. *et al.* Trimethylsilyl-terminated oligo(phenylene ethynylene)s: an approach to single-molecule junctions with covalent Au–C σ-bonds. *J. Am. Chem. Soc.* **134**, 19425–19431 (2012).
73. Wuts, P. G. M. & Greene, T. W. *Greene's Protective Groups in Organic Synthesis* 4th edn (Wiley, 2006).
74. Nagahara, L. A., Thundat, T. & Lindsay, S. M. Preparation and characterization of STM tips for electrochemical studies. *Rev. Sci. Instrum.* **60**, 3128–3130 (1989).
75. Saby, C., Ortiz, B., Champagne, G. Y. & Be, D. Electrochemical modification of glassy carbon electrode using aromatic diazonium salts. 1. Blocking effect of 4-nitrophenyl and 4-carboxyphenyl groups. *Langmuir* **7463**, 6805–6813 (1997).
76. Hines, T. *et al.* Controlling formation of single-molecule junctions by electrochemical reduction of diazonium terminal groups. *J. Am. Chem. Soc.* **135**, 3319–3322 (2013).
77. Patai, S. *Diazonium Diazo Groups* Vol. 1 (Wiley, 1978).
78. Pearson, R. G. Hard and soft acids and bases. *J. Am. Chem. Soc.* **85**, 3533–3539 (1963).
79. Ullmann, F. & Bielecki, J. Ueber synthesen in der biphenylreihe. *Ber. Dtsch. Chem. Ges.* **34**, 2174–2185 (1901).
80. Cai, J. *et al.* Atomically precise bottom-up fabrication of graphene nanoribbons. *Nature* **466**, 470–473 (2010).
81. Koch, M., Ample, F., Joachim, C. & Grill, L. Voltage-dependent conductance of a single graphene nanoribbon. *Nat. Nanotechnol.* **7**, 713–718 (2012).
82. Nguyen, S. & Grubbs, R. H. Syntheses and activities of new single-component, ruthenium-based olefin metathesis catalysts. *J. Am. Chem. Soc.* **115**, 9858–9859 (1993).
83. Tulevski, G. S., Myers, M. B., Hybertsen, M. S., Steigerwald, M. L. & Nuckolls, C. Formation of catalytic metal–molecule contacts. *Science* **309**, 591–594 (2005).
84. Kim, T., Vāzquez, H., Hybertsen, M. S. & Venkataraman, L. Conductance of molecular junctions formed with silver electrodes. *Nano Lett.* **13**, 3358–3364 (2013).
85. Kaneko, S., Nakazumi, T. & Kiguchi, M. Fabrication of a well-defined single benzene molecule junction using Ag electrodes. *J. Phys. Chem. Lett.* **1**, 3520–3523 (2010).
86. Haick, H., Ghabboun, J. & Cahen, D. Pd versus Au as evaporated metal contacts to molecules. *Appl. Phys. Lett.* **86**, 2004–2006 (2005).
87. Kiguchi, M. *et al.* Highly conductive molecular junctions based on direct binding of benzene to platinum electrodes. *Phys. Rev. Lett.* **101**, 046801 (2008).
88. Kim, Y. *et al.* Conductance and vibrational states of single-molecule junctions controlled by mechanical stretching and material variation. *Phys. Rev. Lett.* **106**, 196804 (2011).
89. Yelin, T. *et al.* Atomically wired molecular junctions: connecting a single organic molecule by chains of metal atoms. *Nano Lett.* **13**, 1956–1961 (2013).
90. Ko, C. H., Huang, M. J., Fu, M. D. & Chen, C. H. Superior contact for single-molecule conductance: electronic coupling of thiolate and isothiocyanate on Pt, Pd, and Au. *J. Am. Chem. Soc.* **132**, 756–764 (2010).
91. Seminario, J. M., De La Cruz, C. E. & Derosa, P. A. A. Theoretical analysis of metal–molecule contacts. *J. Am. Chem. Soc.* **123**, 5616–5617 (2001).
92. Adak, O., Korytār, R., Joe, A. Y., Evers, F. & Venkataraman, L. Impact of electrode density of states on transport through pyridine-linked single molecule junctions. *Nano Lett.* **15**, 3716–3722 (2015).
93. Schmaus, S. *et al.* Giant magnetoresistance through a single molecule. *Nat. Nanotechnol.* **6**, 185–189 (2011).
94. Wende, H. *et al.* Substrate-induced magnetic ordering and switching of iron porphyrin molecules. *Nat. Mater.* **6**, 516–520 (2007).
95. Iacovita, C. *et al.* Visualizing the spin of individual cobalt–phthalocyanine molecules. *Phys. Rev. Lett.* **101**, 40–43 (2008).
96. Metzger, R. M. Unimolecular Electronics. *Chem. Rev.* **115**, 5056–5115 (2015).
97. Luo, L., Choi, S. H. & Frisbie, C. D. Probing hopping conduction in conjugated molecular wires connected to metal electrodes. *Chem. Mater.* **23**, 631–645 (2011).
98. Miller, R. D. & Michl, J. Polysilane high polymers. *Chem. Rev.* **89**, 1359–1410 (1989).
99. Chen, W. *et al.* Aromaticity decreases single-molecule junction conductance. *J. Am. Chem. Soc.* **136**, 918–920 (2014).
100. Wudl, F., Kobayashi, M. & Heeger, A. J. Poly(isothianaphthene). *J. Org. Chem.* **49**, 3382–3384 (1984).
101. Douglas, J. D. *et al.* Functionalized isothianaphthene monomers that promote quinoidal character in donor–acceptor copolymers for organic photovoltaics. *Macromolecules* **45**, 4069–4074 (2012).

102. Breslow, R. & Foss Jr, F. W. Charge transport in nanoscale aromatic and antiaromatic systems. *J. Phys. Condens. Matter* **20**, 374104 (2008).
103. Venkataraman, L. *et al.* Electronics and chemistry: varying single-molecule junction conductance using chemical substituents. *Nano Lett.* **7**, 502–506 (2007).
104. Hammett, L. P. Effect of structure upon the reactions of organic compounds. Benzene derivatives. *J. Am. Chem. Soc.* **59**, 96–103 (1937).
105. Malen, J. A. *et al.* The nature of transport variations in molecular heterojunction electronics. *Nano Lett.* **9**, 3406–3412 (2009).
106. Vonlanthen, D. *et al.* Chemically controlled conductivity: torsion-angle dependence in a single-molecule biphenyldithiol junction. *Angew. Chem. Int. Ed. Engl.* **48**, 8886–8890 (2009).
107. Mishchenko, A. *et al.* Single-molecule junctions based on nitrile-terminated biphenyls: a promising new anchoring group. *J. Am. Chem. Soc.* **133**, 184–187 (2011).
108. Jan van der Molen, S. & Liljeroth, P. Charge transport through molecular switches. *J. Phys. Condens. Matter* **22**, 133001 (2010).
109. Sun, L. *et al.* Single-molecule electronics: from chemical design to functional devices. *Chem. Soc. Rev.* **43**, 7378–7411 (2014).
110. Lara-Avila, S. *et al.* Bianthrone in a single-molecule junction: conductance switching with a bistable molecule facilitated by image charge effects. *J. Phys. Chem. C* **114**, 20686–20695 (2010).
111. Dulić, D. *et al.* One-way optoelectronic switching of photochromic molecules on gold. *Phys. Rev. Lett.* **91**, 207402 (2003).
112. van der Molen, S. J. *et al.* Light-controlled conductance switching of ordered metal–molecule–metal devices. *Nano Lett.* **9**, 76–80 (2009).
113. Darwish, N., Aragonès, A. C., Darwish, T., Ciampi, S. & Díez-Pérez, I. Multi-responsive photo- and chemo-electrical single-molecule switches. *Nano Lett.* **14**, 7064–7070 (2014).
114. Li, Z. *et al.* Single-molecule sensing of environmental pH — an STM break junction and NEGF-DFT approach. *Angew. Chem. Int. Ed. Engl.* **53**, 1098–1102 (2014).
115. Roldan, D. *et al.* Charge transport in photoswitchable dimethyldihydropyrene-type single-molecule junctions. *J. Am. Chem. Soc.* **135**, 5974–5977 (2013).
116. Liljeroth, P., Repp, J. & Meyer, G. Current-induced hydrogen tautomerization and conductance switching of naphthalocyanine molecules. *Science* **317**, 1203–1206 (2007).
117. Auwärter, W. *et al.* A surface-anchored molecular four-level conductance switch based on single proton transfer. *Nat. Nanotechnol.* **7**, 41–46 (2012).
118. Lörtscher, E., Ciszek, J. W., Tour, J. & Riel, H. Reversible and controllable switching of a single-molecule junction. *Small* **2**, 973–977 (2006).
119. Baer, R. & Neuhauser, D. Phase coherent electronics: a molecular switch based on quantum interference. *J. Am. Chem. Soc.* **124**, 4200–4201 (2002).
120. Cardamone, D. M., Stafford, C. A. & Mazumdar, S. Controlling quantum transport through a single molecule. *Nano Lett.* **6**, 2422–2426 (2006).
121. Hod, O., Baer, R. & Rabani, E. A. Parallel electromagnetic molecular logic gate. *J. Am. Chem. Soc.* **127**, 1648–1649 (2005).
122. Vazquez, H. *et al.* Probing the conductance superposition law in single-molecule circuits with parallel paths. *Nat. Nanotechnol.* **7**, 663–667 (2012).
123. Guédon, C. M. *et al.* Observation of quantum interference in molecular charge transport. *Nat. Nanotechnol.* **7**, 305–309 (2012).
124. Rabache, V. *et al.* Direct observation of large quantum interference effect in anthraquinone solid-state junctions. *J. Am. Chem. Soc.* **135**, 10218–10221 (2013).
125. Darwish, N. *et al.* Observation of electrochemically controlled quantum interference in a single anthraquinone-based norbornylogous bridge molecule. *Angew. Chem. Int. Ed. Engl.* **51**, 3203–3206 (2012).
126. Baghernejad, M. *et al.* Electrochemical control of single-molecule conductance by fermi-level tuning and conjugation switching. *J. Am. Chem. Soc.* **136**, 17922–17925 (2014).
127. Solomon, G. C., Herrmann, C., Hansen, T., Mujica, V. & Ratner, M. A. Exploring local currents in molecular junctions. *Nat. Chem.* **2**, 223–228 (2010).
128. Solomon, G. C. *et al.* Quantum interference in acyclic systems: conductance of cross-conjugated molecules. *J. Am. Chem. Soc.* **130**, 17301–17308 (2008).
129. Phelan, N. F. & Orchin, M. Cross conjugation. *J. Chem. Educ.* **45**, 633–637 (1968).
130. Klausen, R. S. *et al.* Evaluating atomic components in fluorene wires. *Chem. Sci.* **5**, 1561–1564 (2014).
131. Yoshizawa, K. An orbital rule for electron transport in molecules. *Acc. Chem. Res.* **45**, 1612–1621 (2012).
132. Tsuji, Y. & Hoffmann, R. Frontier orbital control of molecular conductance and its switching. *Angew. Chem. Int. Ed. Engl.* **53**, 4093–4097 (2014).
133. Coulson, C. A. & Rushbrooke, G. S. Note on the method of molecular orbitals. *Math. Proc. Cambridge Philos. Soc.* **36**, 193–200 (1940).
134. Markussen, T., Stadler, R. & Thygesen, K. S. The relation between structure and quantum interference in single molecule junctions. *Nano Lett.* **10**, 4260–4265 (2010).
135. Li, E. Y. & Marzari, N. Conductance switching and many-valued logic in porphyrin assemblies. *J. Phys. Chem. Lett.* **4**, 3039–3044 (2013).
136. Qian, G., Saha, S. & Lewis, K. M. Two-state conductance in single Zn porphyrin molecular junctions. *Appl. Phys. Lett.* **96**, 243107 (2010).
137. Li, X., Staykov, A. & Yoshizawa, K. Orbital views of the electron transport through polycyclic aromatic hydrocarbons with different molecular sizes and edge type structures. *J. Phys. Chem. C* **114**, 9997–10003 (2010).
138. Yamada, R., Kumazawa, H., Noutoshi, T., Tanaka, S. & Tada, H. Electrical conductance of oligothiophene molecular wires. *Nano Lett.* **8**, 1237–1240 (2008).
139. Reuter, M. G. & Hansen, T. Finding destructive interference features in molecular transport junctions. *J. Chem. Phys.* **141**, 181103 (2014).
140. Bartels, L. Tailoring molecular layers at metal surfaces. *Nat. Chem.* **2**, 87–95 (2010).
141. Maggio, E., Solomon, G. C. & Troisi, A. Exploiting quantum interference in dye sensitized solar cells. *ACS Nano* **8**, 409–418 (2014).
142. Bergfield, J. P., Heitzer, H. M., Van Dyck, C., Marks, T. J. & Ratner, M. A. Harnessing quantum interference in molecular dielectric materials. *ACS Nano* **9**, 6412–6418 (2015).
143. Landauer, R. Spatial variation of currents and fields due to localized scatterers in metallic conduction. *IBM J. Res. Dev.* **1**, 223–231 (1957).
144. Büttiker, M., Imry, Y., Landauer, R. & Pinhas, S. Generalized many-channel conductance formula with application to small rings. *Phys. Rev. B* **31**, 6207–6215 (1985).
145. He, J. *et al.* Electronic decay constant of carotenoid polyenes from single-molecule measurements. *J. Am. Chem. Soc.* **127**, 1384–1385 (2005).
146. Lu, Q. *et al.* From tunneling to hopping: a comprehensive investigation of charge transport mechanism in molecular junctions based on oligo(*p*-phenylene ethynylene)s. *ACS Nano* **3**, 3861–3868 (2009).
147. Kaliginedi, V. *et al.* Correlations between molecular structure and single-junction conductance: a case study with oligo(phenylene-ethynylene)-type wires. *J. Am. Chem. Soc.* **134**, 5262–5275 (2012).
148. Capozzi, B. *et al.* Length-dependent conductance of oligothiophenes. *J. Am. Chem. Soc.* **136**, 10486–10492 (2014).
149. Hines, T. *et al.* Transition from tunneling to hopping in single molecular junctions by measuring length and temperature dependence. *J. Am. Chem. Soc.* **132**, 11658–11664 (2010).

Acknowledgements
T.A.S. is supported by an NSF Graduate Research Fellowship under grant no. 11-44155. The authors thank the NSF for support under grant no. CHE-1404922.

Competing interests statement
The authors declare no competing interests.